

GEO PERSIA



Accepted Manuscript

Hydrogeochemistry and groundwater origin in the Sarduiyeh area, Iran

Reza Jahanshahi, Nozhat Mahmoodinejad, Sepideh Mali

DOI: 10.22059/GEOPE.2025.390781.648810

Receive Date: 19 February 2025

Revise Date: 15 March 2025

Accept Date: 17 March 2025

Accepted Manuscript

Hydrogeochemistry and groundwater origin in the Sarduiyeh area, Iran

Reza Jahanshahi ^{1,*}, Nozhat Mahmoodinejad ², Sepideh Mali ³

¹ School of Geology, College of Science, University of Tehran, Tehran, Iran

² Faculty of Science, University of Sistan and Baluchestan, Zahedan, Iran

³ Faculty of Geosciences, Shahrood University of Technology, Shahrood, Iran

Received: 19 February 2025, Revised: 15 March 2025, Accepted: 17 March 2025

© University of Tehran

Abstract

In this study, hydrogeochemistry, the origin of the water resources, and geothermometry were investigated in the study area. Water resources at 43 points included 22 qanats, 3 wells, 12 cold springs, 2 thermal springs and 4 rivers. Based on the results, there were four dominant water types in the study area: Na-SO₄, Na-HCO₃, Na-Cl and Ca-HCO₃ in the study area. The electrical conductivity (EC) in the groundwater varied between 1643 and 133 $\mu\text{S}/\text{cm}$. Most water samples were supersaturated with respect to calcite and dolomite, while all samples were undersaturated with respect to gypsum and halite. According to ion ratios, calcium can also be derived from sources such as calcite, gypsum, dolomite, and silicates. The thermal springs in the area exhibited a different chemical composition compared to other water samples and had the highest EC and sulfate concentration. According to stable isotopes ($\delta^{18}\text{O}$ and $\delta^2\text{H}$), the source of cold-water springs and qanat was related to rainfall in the study area and re-evaporation has likely occurred in the precipitation. Additionally, the source of the thermal springs was probably related to the precipitation, and the possibility of mixing magmatic water with groundwater for the generation of thermal springs in the study area is low. Based on the geothermometry of the CCG method in hot springs, the thermal reservoir temperature was estimated about 165 °C, and the depth of this reservoir was likely located at 2500-3900 m.

Keywords: Water Mixing, Saturation Index, Stable Isotopes, Geothermometry.

Introduction

Groundwater is increasingly recognized as a preferred source of drinking water in arid and semi-arid regions. This preference stems from its low treatment needs, widespread availability, and ability to manage significant fluctuations in rainfall, as well as the water demands that arise during droughts and when surface water resources exceed sustainable limits (Shojaei Baghini et al., 2020; Loh et al., 2020). A thorough groundwater assessment must take into account the various factors and processes that affect groundwater chemistry over time and across different locations. This understanding is essential for the effective management of the resource. To this end, researchers have implemented various strategies to evaluate the different sources of variation in groundwater chemistry (Telahigue et al., 2018; Sunkari et al., 2019; Mali et al., 2022). Recently, advanced geostatistical techniques have played a leading role in this area, particularly in hydrochemical studies (Nakhaie Sarvedani et al., 2022). These methods have been utilized to characterize groundwater flow patterns, differentiate hydrochemical facies, predict conditions at unsampled sites, create statistical models, pinpoint sources of variation, and describe the evolution of groundwater (Ahmadi et al., 2018; Sunkari et al., 2019; Loh et al., 2020). The chemical characteristics of groundwater are crucial for evaluating and

* Corresponding author e-mail: rezajahanshahi@ut.ac.ir

categorizing water quality. Several factors influence groundwater quality, including the geology of the area, the extent of chemical weathering of different rock types, the quality of the recharge water, and the interactions between water and rock (Giridharan et al. 2008; Aly 2015; Aghazadeh et al., 2017). Many recent studies have concentrated on examining the natural concentrations of various ions and metals in groundwater. The goal is to distinguish between anthropogenic and natural sources that impact groundwater quality and to understand the interactions occurring within the aquifer (Jacinta et al. 2016; Ehya and Marbouti 2016; Sethy et al. 2016; Aghazadeh et al., 2017).

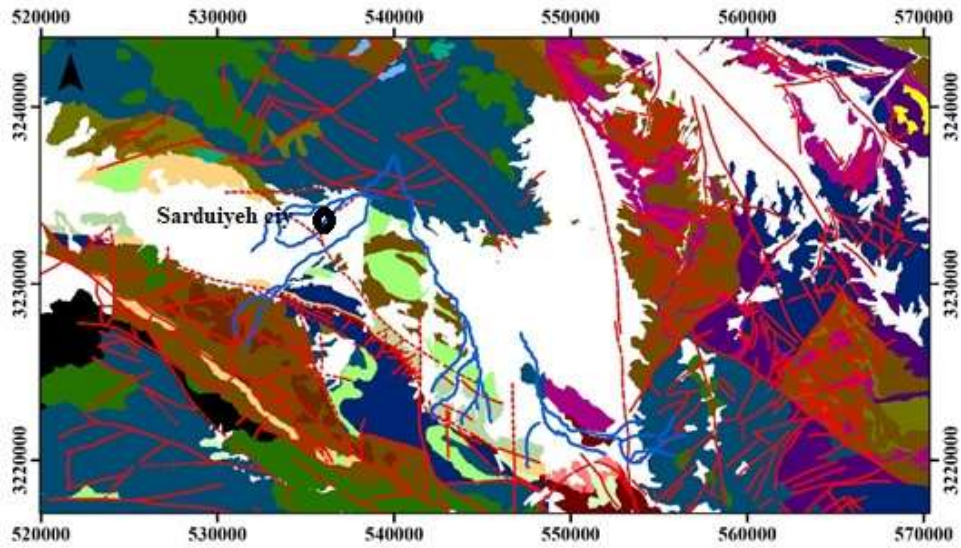
In this research, various methods for assessing groundwater were implemented for specific purposes in the Sarduiyeh region, particularly in light of increasing development of urbanization, agriculture, and the mining industry in this area. Investigating the hydrogeochemical and natural isotopic conditions of the region before they undergo adverse changes due to anthropogenic factors is very important for the foundation of quality management plans for water resources. Hydrogeochemical and isotopic studies of water are essential for understanding the effective factors in the origin and degradation of surface and underground water resources.

Study area

The Sarduiyeh plain is located to the north of Jiroft city in Kerman province, Iran. In the study area, the geological formations include rocks of basalt, andesite, and pyroclastics belonging to the Lower Eocene. The hard rock formations in the Sarduiyeh area belong to different geological periods and exhibit a wide lithological diversity. According to Dimitriyevic et al. (1973) and the geological map (Fig. 1), the hard rocks of the Tertiary period occupy more than 70% of the area. The largest rock unit consists of rhyodacite, agglomerate, and related pyroclastics, which cover a northwest-southeast trend; another outcrop can be seen in the northeast of the study area. Additionally, the largest area covered by the agglomerate unit consists of acid tuffs with some andesitic basalt lava. Other Eocene volcanic rock units are distributed in the north and south of the study area. Conglomerate, tuffite sandstone, turbidite sediments, and Quaternary sediments are also present. In this area, there is a thermal spring with an average temperature of 48 °C, which has one of the highest electrical conductivities (EC) of groundwater in the study area. The general direction of groundwater flow in the study area is from southeast to north and northwest (Fig. 2), following the topography of the ground surface. Groundwater moves through formations of Cenozoic and Mesozoic (siltstone, conglomerate, sandstone, and limestone) and Quaternary deposits.

Materials and methods

In total, 43 water samples from groundwater (cold and thermal springs, wells and qanats) and surface water (Fig. 3) were collected in washed polyethylene bottles for hydrogeochemical and stable isotope analyses (Table 1). It is necessary to mention that to separate the suspended particles, water samples were filtered with 0.45 µm pore-sized filters. The pH, temperature, electrical conductivity, and alkalinity were obtained in situ. To analyze the major cation, the water samples were treated with a 65% HNO₃ solution. Concentration of Cl⁻ and HCO₃⁻ were analyzed by titration methods, SO₄²⁻ was analyzed using an IC device (HP Agilent 4500), and other elements were analyzed using an ICP-MC device (HP Agilent 4500). The analyses of stable isotopes δ¹⁸O and δ²H were performed by an OA-ICOS device using a liquid water isotope analyzer. The results were expressed according to the VSMOW international standard with the analytical precisions of ±0.03‰ and ±1.20‰ for δD and δ¹⁸O, respectively.



Legend

Sedimentary rock units

- Alluvium and gravel fans
- Siltstone
- Talus cones
- Shale and marl
- Limestone
- Conglomerate
- Calcareous terraces
- Biomicrite
- River
- Fault

Igneous rock units

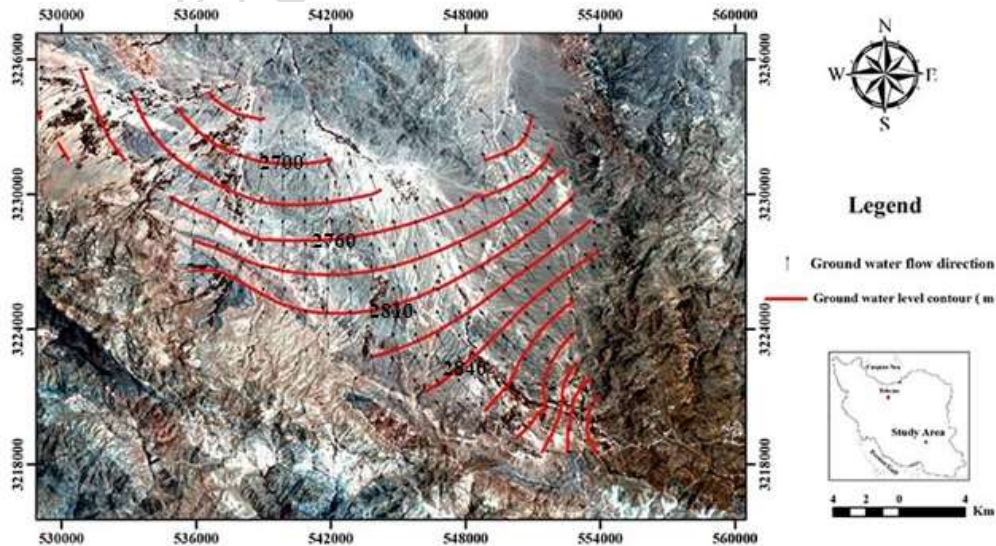
- Tuffaceous sandstone
- Acidic and basic lava
- Acidic pyroclastics
- Trachy_andesite
- Agglomerate
- Pyroclastics
- Granodiorite
- Rhyodacite



- Rhyolite
- Dacite
- Andesite

Fault, active during Quaternary

Figure 1. Geological map of the study area



Legend

- Ground water flow direction
- Ground water level contour (m)

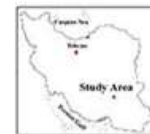


Figure 2. Groundwater flow direction in the study area

Table 1. Physicochemical properties of the water resources in the study area (EC in $\mu\text{S}/\text{cm}$, ions concentrations in mg/L , and stable isotopes δD and $\delta^{18}\text{O}$ in ‰ VSMOW)

Name	EC	pH	Na	K	Ca	Mg	HCO ₃	Cl	SO ₄	18O	dD
Q1	340	8.23	18	2	49	7.2	178.1	10	22	-	-
Q2	277	7.99	16	1	42.5	5.9	174.2	10	17.5	-	-
Q3	496	8.22	44	1	51	10.3	188.2	22	62	-	-
Q4	960	7.15	132	1.5	64.7	14.3	203.2	100	160	-	-
Q5	552	8.12	48	1	60.4	11.2	218.2	30	56	-	-
Q6	1421	8.05	206	4	78.2	18.9	244.2	154	300	-	-
Q7	695	8.09	100	1.5	42.8	8.9	151.1	44	162	-	-
Q8	1111	8.17	183	3	52.3	11.4	177.2	170	162	-	-
Q9	365	7.89	11	0.5	52.6	8.7	192.1	9	18	-	-
Q10	268	8.35	7	0.5	39.2	5.7	133.1	8	12	-	-
Q11	308	8.01	11	0.5	42.2	6.1	139.1	8	18	-	-
Q12	495	7.59	13	0.5	88.4	11.3	298.2	11	23	-	-
Q13	500	7.39	8	1	89	12.1	294.2	9	17	-	-
Q14	573	7.39	17	1	77.7	14.8	250.2	19	57	-	-
Q15	667	7.43	27	1.5	94.3	16.4	294.3	20	80	-	-
Q16	605	7.69	28	1	96	16.3	294.2	19	70	-	-
Q17	461	7.64	21	1	72.9	14	293.2	13	35	-	-
Q18	368	7.69	13	0.5	75.5	11.8	250.2	11.4	35	-	-
Q19	355	7.65	11	0.5	66.7	9.6	232.2	6.5	22	-	-
Q20	359	7.74	12	1	61.9	9.4	214.1	9	32	-	-
Q21	361	7.56	7	0.5	69.2	7.5	174.2	9.7	53	-5.42	-27.09
Q22	463	7.57	18	1	79.7	9.1	249.2	15	36	-	-
R1	527	8.02	24	1	87.8	16.6	235.2	13	104	-	-
R2	674	7.71	32	1	88.5	20.2	282.2	33	67	-	-
R3	768	7.41	43	1.5	109.5	28.8	334.3	30	208	-	-
R4	133	7.68	5	0.5	25	2.8	80.1	8.5	10.5	-	-
SP1	458	7.95	23	2	83	12	269.2	15	67	-4.96	-25.63
SP2	406	7.95	18	1.5	56.6	8.8	203.2	11	18	-	-
SP3	295	8.11	17	1	38.8	5.1	149.1	10	19	-	-
SP4	415	8	23	1	56.6	8.6	214.2	10.3	19.3	-	-
SP5	478	8.2	29	2	73.5	11.6	270.2	17.5	34	-	-
SP6	482	8.17	27	1.5	63.5	10.9	205.2	21.5	41	-	-
SP7	535	8.08	70	1.5	40.4	8.5	204.1	23	67	-	-
SP8	708	7.94	99	2	50.7	11.3	208.1	31	140	-5.46	-31.72
SP9	508	7.35	10	0.5	85.3	9.9	261.2	10	60	-5.11	-26.33
SP10	579	8.2	41	1	56.8	20.2	239.2	23	120	-	-
SP11	635	7.86	48	1	57	11.8	198.2	35	98	-3.69	-25.81
SP12	746	7.54	35	1	103.6	17.2	283.3	21	130	-	-
SPg1	1595	8.05	294	7	49	0.2	119.1	203	424	-	-
SPg2	1643	8.48	299	7	49	0.2	110.1	215	450	-6.31	-34.57
W1	739	7.68	30	1	110	19.4	320.3	21	110	-	-
W2	1183	7.61	67	2	133	47.5	370.4	50	324	-	-
W3	671	7.69	36	1	75.4	18.5	270.2	22	120	-	-

Results and discussion

Hydrochemistry characteristics

The EC in the groundwater resources of the study area varied between 133 to 1643 $\mu\text{S}/\text{cm}$ increasing from the south and west to the north and east of the study area. Based on the piper diagram, four types of water were identified as Ca-HCO₃, Na-HCO₃, Na-SO₄ and Na-Cl in the groundwater of the study area (Fig. 4). In general, the dominant anions in the water samples changed from bicarbonate to sulfate, while the dominant cation changed from Ca to Na. However, most of the water samples plotted in the temporary hardness (carbonate hardness) part of the piper diagram.

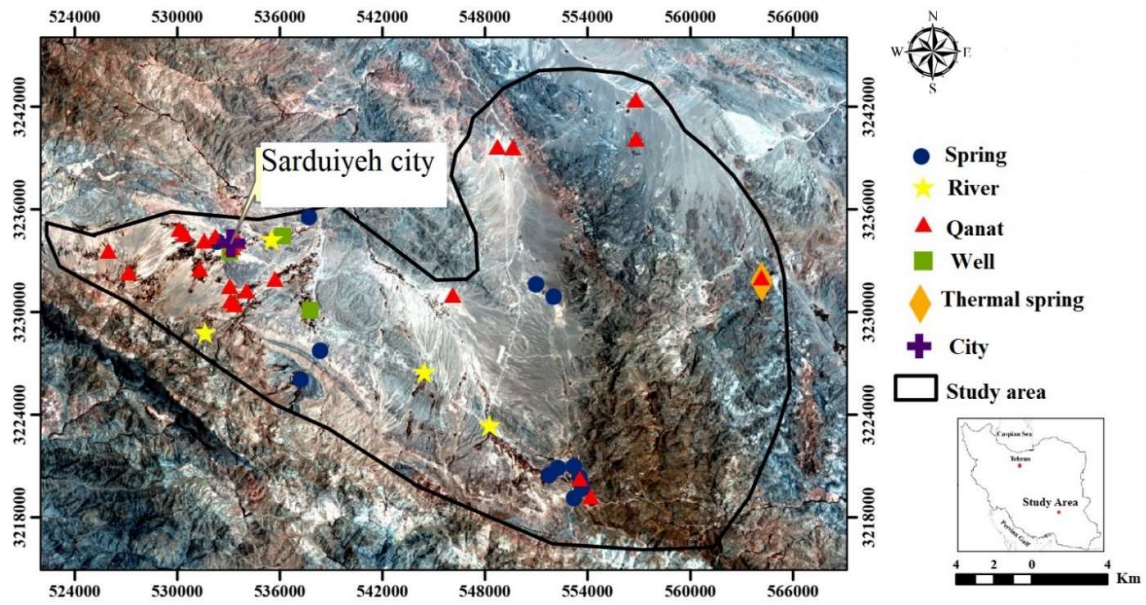


Figure 3. the location of water sampling points

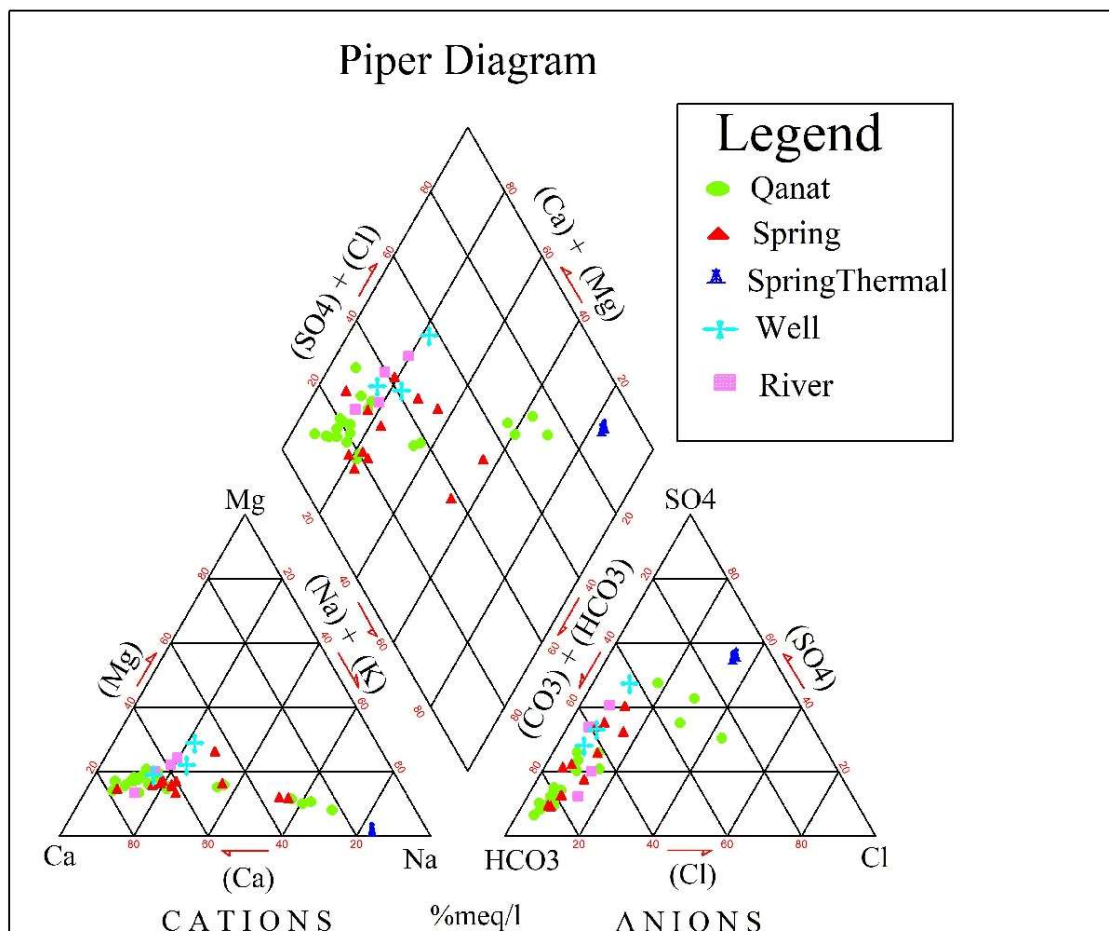


Figure 4. Piper diagram for water samples in the study area

According to the molar ratio of Na/Cl in Fig. 5a, most of the water samples are plotted above 1, which indicates that in addition to halite mineral dissolution, the source of Na could be the weathering of Na-bearing silicate minerals and cation exchange reactions. Additionally, in general, this graph shows that as salinity (Cl^-) increases, this ratio decreases in the groundwater of the study area. Analyzing the molar ratio of Ca and HCO_3^- in Fig. 5b, it is observed that some water samples fall on the 1:2 line, suggesting that the calcium source is likely the dissolution of calcite mineral. However, a few samples do not fall on the 1:2 line, indicating that calcite is not the sole source of calcium. Moving on to molar ratio of calcium to magnesium in Fig. 5c, it is noted that the samples do not align with the dissolution line of dolomite, and generally the amount of calcium is higher than magnesium. This suggests that some of the Ca may be entering the groundwater from another source, or some of the Mg may be sinking from the groundwater due to processes like cation exchange or the deposition of Mg-bearing minerals. To investigate the dissolution of gypsum, the molar ratio of 1:1 for Ca and SO_4 is considered in Fig. 5d. This indicates that the dissolution of gypsum occurred in water samples Q4 and W2. Water samples Spg1, Spg2, Q6, Q7, Q8 and Sp8 were located above the 1:1 ratio line, suggesting that Ca may be obtained from sources other than gypsum such as the dissolution of calcite, dolomite and Ca-bearing silicate minerals. The two hot springs (Spg1 and Spg2) were notably far from the gypsum dissolution line. In the samples below the 1:1 ratio, the concentration of sulfate was higher than calcium, indicating that Ca is likely being removed from the solution due to mineral deposition or ion exchange. If the water samples are located above the 3:1 line for the molar ratio of $\text{SO}_4 + \text{HCO}_3^-$: Ca, it suggests weathering of silicates (Fig. 5e).

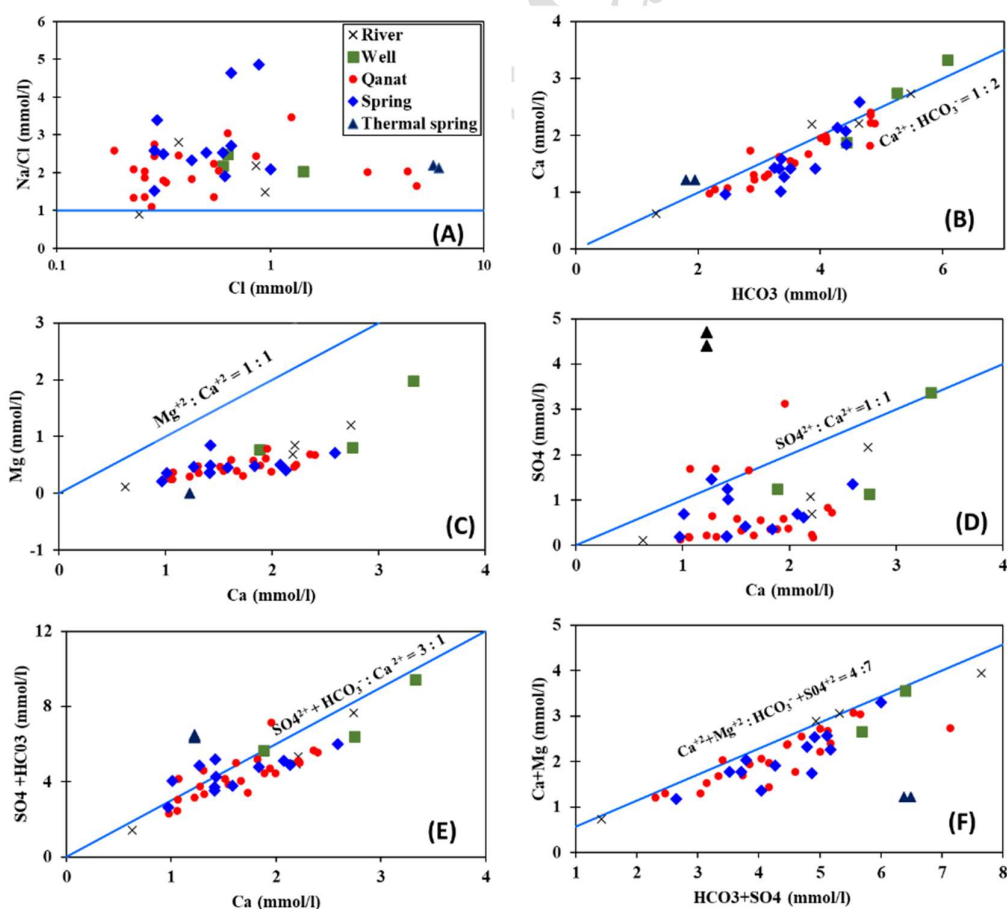


Figure 5. The molar ratio of ions

This indicates that hot springs were likely influenced by silicate minerals more than other water sources. Finally, according to Fig. 4f, it is possible that simultaneous dissolution of gypsum, calcite, and dolomite minerals occurred in the water resources of the study area.

Ion Li is commonly used as a suitable tracer for the evolution of evaporation processes in primary solutions. For this purpose, water samples collected from the study area were plotted on a Li/Cl versus Br/Cl plot (Bagheri et al., 2014) (Fig. 6). As can be seen, the samples are located in the salinity range resulting from the evaporite formations.

The negative saturation index of gypsum and halite minerals in surface and groundwater samples of the region indicates that these minerals are undersaturated. The calcite saturation index is positive in all cold and hot spring, qanat and river water samples except for Q4 and R4 samples. The dolomite saturation index is also positive in most points and is negative in 7 qanat samples, 2 river samples and samples spring Sp9 and hot spring Spg1. The increase in the concentration of Ca and Mg from weathering of feldspar minerals and other calcium and magnesium-containing minerals has caused the groundwater samples to be supersaturated with respect to calcite and dolomite. The saturation index of the minerals against EC is showing in Fig. 7, show that with increasing salinity, the saturation index of dolomite, calcite, gypsum, and halite increased.

Hierarchical cluster analysis

The tree branch diagram or dendrogram resulting from the clustering method of water samples in the study area is shown in Fig. 8. The parameters used in this analysis are electrical conductivity, major ions and pH. A similarity value of 0.993-0.994 was considered to measure the difference between groups. According to the shape of the dendrogram, density of groups and chemical composition, the groundwater samples have been divided into three groups. The samples in each cluster have been further divided into subgroups because samples that are similar in several parameters may differ in others.

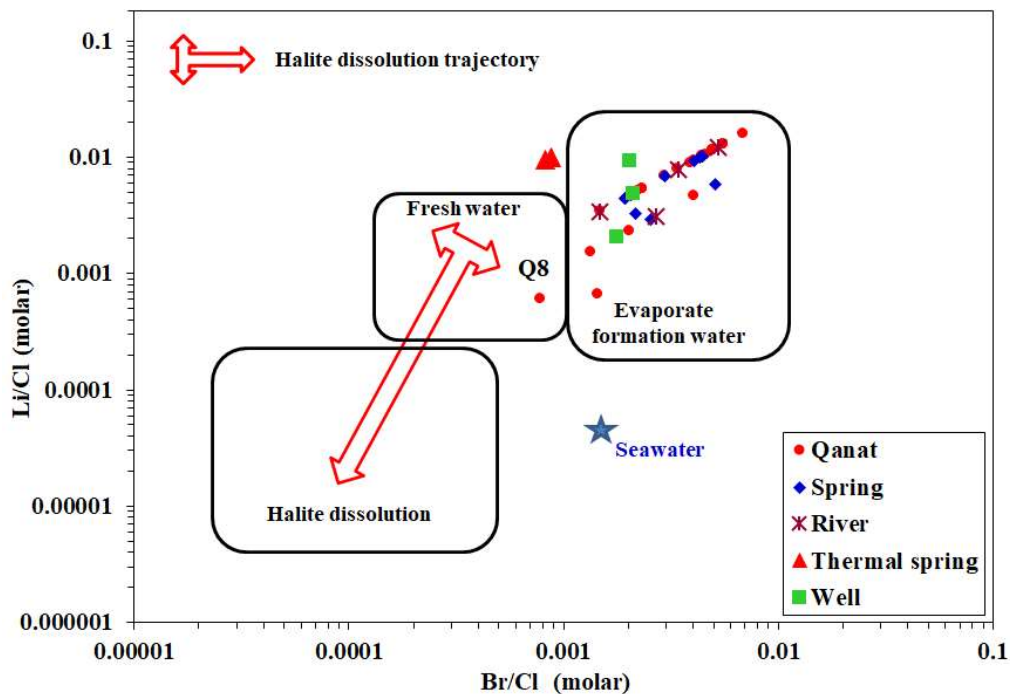


Figure 6. Plot of Li/Cl vs. Br/Cl (Bagheri et al. 2014)

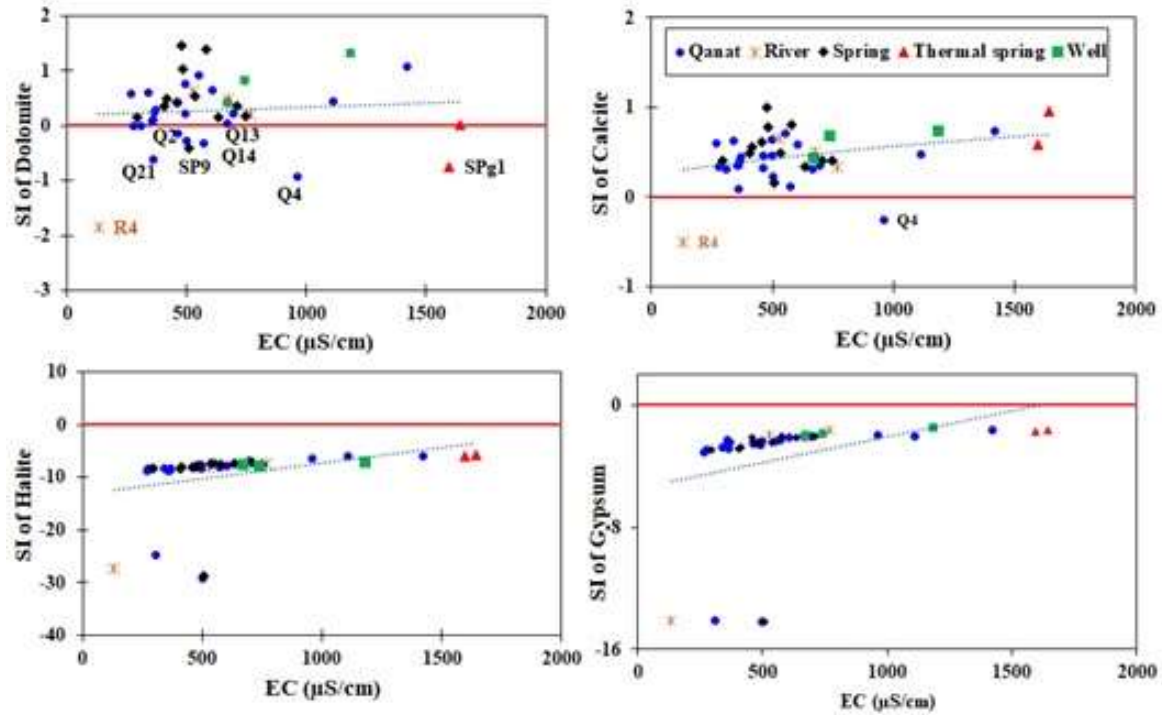


Figure 7. Plot of mineral saturation index vs. EC of the water samples

The samples in cluster 1 have the types Na-SO₄, Na-HCO₃, Na-Cl and Ca-HCO₃. The sample in cluster 2 is only the W2 well water sample and its water type is Ca-HCO₃. According to the analysis of major and minor ions of this sample, its major and minor ions are almost higher than those of other groundwater samples in the study area. Cluster 3 has the Ca-HCO₃ type which includes most of the water source samples. The distribution of this clustering in the area (Fig. 8) also shows that most of the samples are located in cluster 3, which include the southern and western parts of the area, while cluster 1 is mostly located in the northern and eastern parts of the area.

PCO₂ and Ca relation

According to Dreyer (1988), the nonlinear relationship curve between CO₂ pressure and calcium concentration in open system under equilibrium conditions is plotted according to Equation 1 in Fig. 9. To plot the water samples from the study area on this diagram, the pressure of carbon dioxide in water sources was calculated using Henry's law in Equation 2.

$$m_{Ca} = P_{CO_2} \frac{K_1 K_{cal} K_{CO_2}}{4K_2 \gamma Ca^{2+} \gamma^2 HCO_3^-} \quad (1)$$

$$P = KC \quad (2)$$

Where m is the amount of calcium, P is the pressure of carbon dioxide, K_1 is the equilibrium constant of H₂CO₃, K_{cal} is the equilibrium constant of CaCO₃, K_2 is the equilibrium constant of HCO₃⁻, γ is the value of the activity coefficient, K is Henry's Law constant (for carbon dioxide gas equal to 29.4 L.atm/mol) and C is the concentration of CO₂ in water (calculated using inverse geochemical modeling by PHREEQC software).

As shown in Fig. 9, the Ca concentrations of the water samples were above the equilibrium pressure line of CO₂ indicating groundwater resources are supersaturated with respect to Ca. If the relative pressure of dissolved CO₂ in water is greater than the relative pressure of CO₂ in the atmosphere, carbonate deposits are formed in the water. Results showed that in the study

area, the calculated pressures of carbon dioxide in groundwater were higher than the actual pressure of CO₂ in the air (10^{-3.5} atm). Given the pressure of CO₂ in groundwater and the atmosphere, it is almost possible to determine the type of aquifer; If the pressure of dissolved CO₂ is less than the pressure of CO₂ in the atmosphere, the aquifer type will be closed while if the pressure of CO₂ is greater, the aquifer type is unclear and can be both open and closed (Drever, 1988). Hence geological conditions must be investigated. Due to the above, it was not clear whether the hard rock aquifers of the study area were closed or open, and detailed geological studies and aquifers should be reviewed to give an expert opinion on the hard aquifers of the study area with more confidence. Also, the PCO₂ of thermal springs was lower than other water samples. It seems that the solubility of CO₂ has decreased in hot springs due to increasing temperature. On the other hand, due to the longer path of water movement from the earth's surface to the depth and its return (compared to the groundwater movement of cold water springs), carbon dioxide has been consumed because of the dissolution of minerals. Therefore, the amount of this gas in hot springs was less than other water resources.

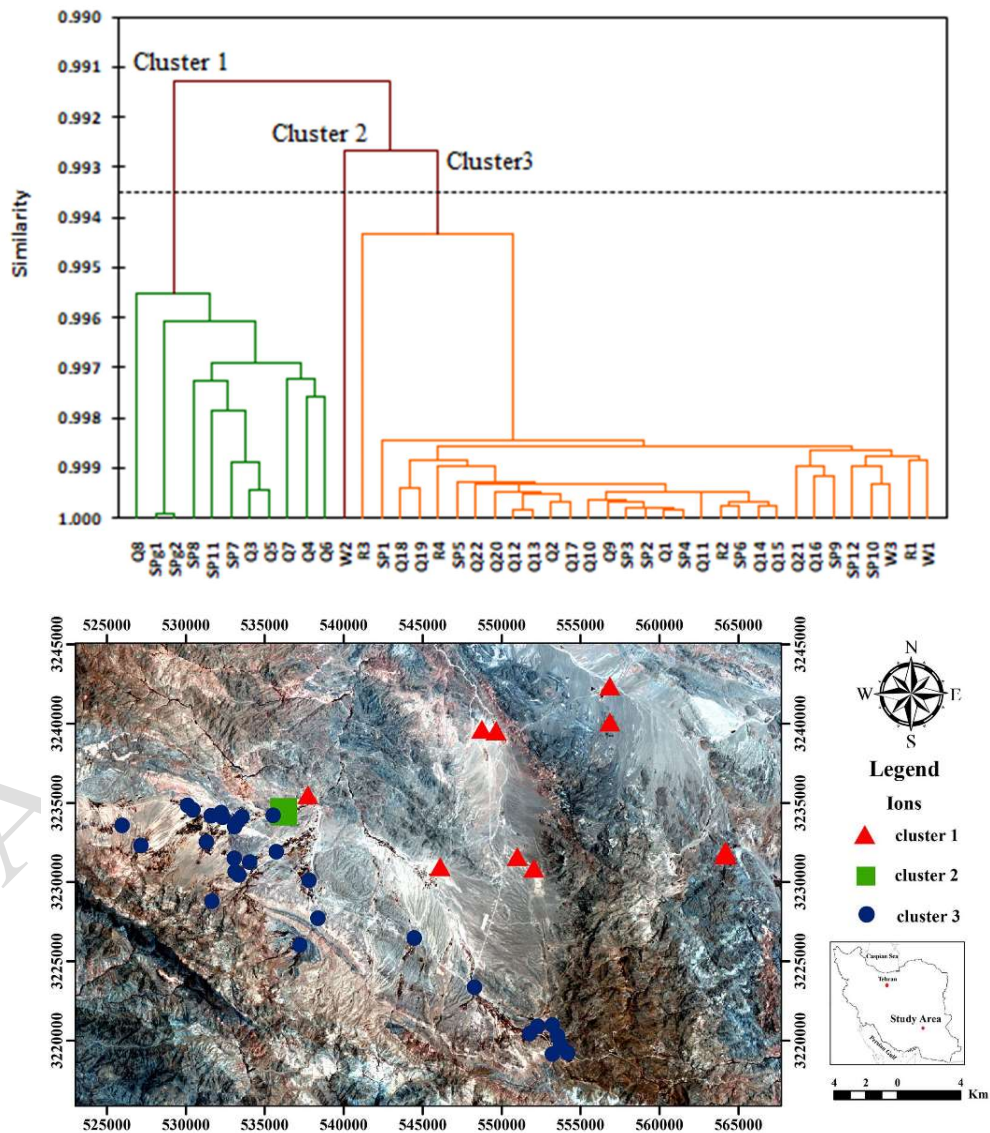


Figure 8. Dendrogram of the Q-mode hierarchical and b distribution map of cluster analysis

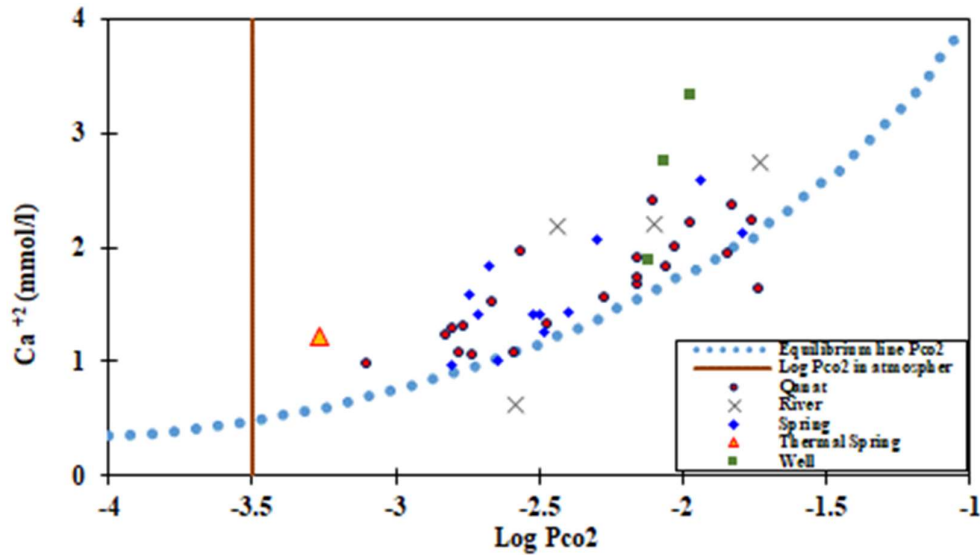


Figure 9. Relationship of PCO₂ - Ca of water samples in the study area

According to Fig. 10 it can be observed that for the same amount of PCO₂, the concentration of Ca in the springs was higher than in the qanats. It is possible that due to the movement of water in the qanat channel from the Mother-well to the outlet of the qanat, some CO₂ is released from the water and some calcium is deposited as calcite or dolomite minerals. Moreover, Fig. 10 indicates that with an increase in dissolved CO₂, more calcium is dissolved in springs than in rivers. Since in the catchment area of the springs, groundwater flows through porous media with a higher residual time compared to river water, this causes the dissolution of minerals to increase while river water moves faster and has less chance of mineral dissolution. Therefore, lower calcium is dissolved in river water than in spring water.

Isotopic characteristics

The $\delta^2\text{H}$ and $\delta^{18}\text{O}$ values in the groundwater ranged from -25.63 to -34.57 ‰ and -3.69 to -6.31 ‰ (VSMOW) respectively in the study area. To investigate the relationship between the $\delta^{18}\text{O}$ and $\delta^2\text{H}$, the global meteoric water line (GWML; Craig 1961) and the local meteoric water line (LWML; Jahanshahi and Zare 2017) were used. The $\delta^{18}\text{O}$ and $\delta^2\text{H}$ of the water samples were plotted in Fig. 11 showing that the isotopic composition of water samples was located to the right and below the GWML and close to LWML. Therefore, the origin of groundwater in springs and qanats is the precipitation of the region and evaporation in the rainfall and groundwater has probably occurred, enriching the isotopic composition of the water samples. Also, thermal springs had the least isotopic enrichment compared to cold water resources in the study area. The origin of these hot springs is probably the current meteoric waters, where factors such as surface evaporation, hot water-rock interaction, and underground evaporation have caused the isotopic composition of them to deviate from precipitation. To investigate the effect of juvenile water on regional water, the average isotopic composition of magmatic water ($\delta^{18}\text{O} = +6 \pm 1$ ‰ and $\delta^2\text{H} = -60 \pm 20$ ‰, Ohmoto (1986)) is plotted on the isotope diagram in Fig. 12. According to the placement of thermal springs outside the mixing area between the average isotopic composition of precipitation and magmatic water, the origin of thermal water cannot result from mixing magmatic water.

According to Bahadori et al (2019) in Iran, air masses generally originating from the Mediterranean Sea, when entering the country from the west and moving to the east, are subjected to isotopic depletion under the influence of the Rayleigh distillation model (Clark and

Fritz, 1997). Therefore, it is expected that precipitation and groundwater resources in the east of the country are more depleted than in the west (Bahadori et al., 2019). Hence, in the study area the relationship between $\delta^{18}\text{O}$ and $\delta^2\text{H}$ values with longitude is considered in Fig. 13, showing a negative relation.

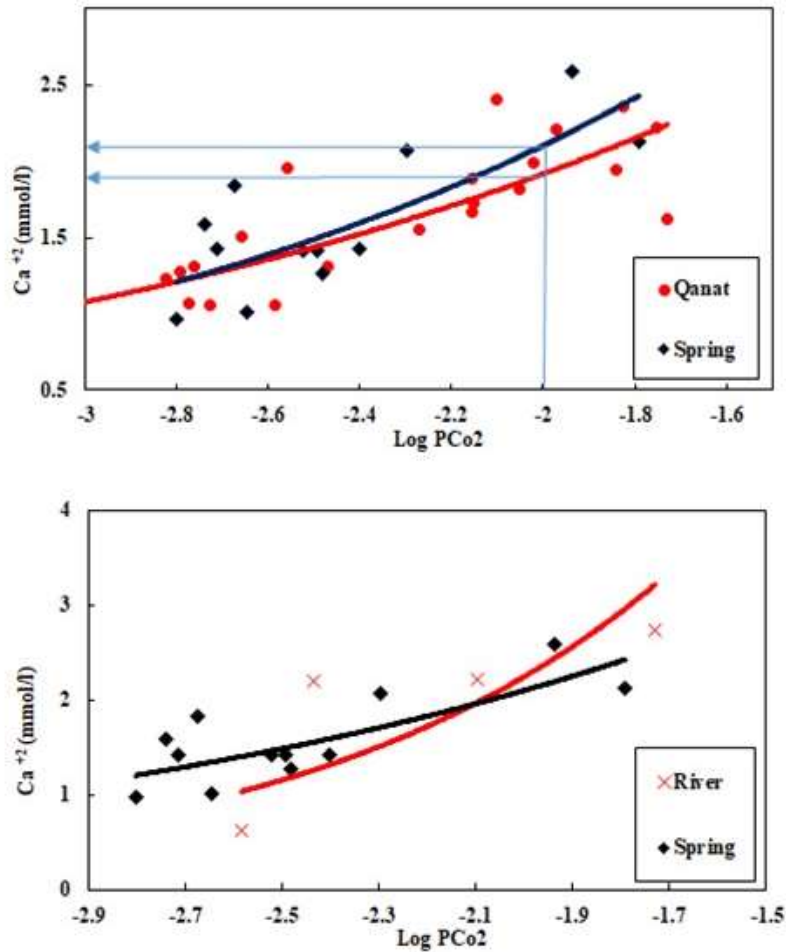


Figure 10. The variation of Log PCO₂ versus calcium concentration, comparison of the qanat and rivers with springs for the water samples of the study area

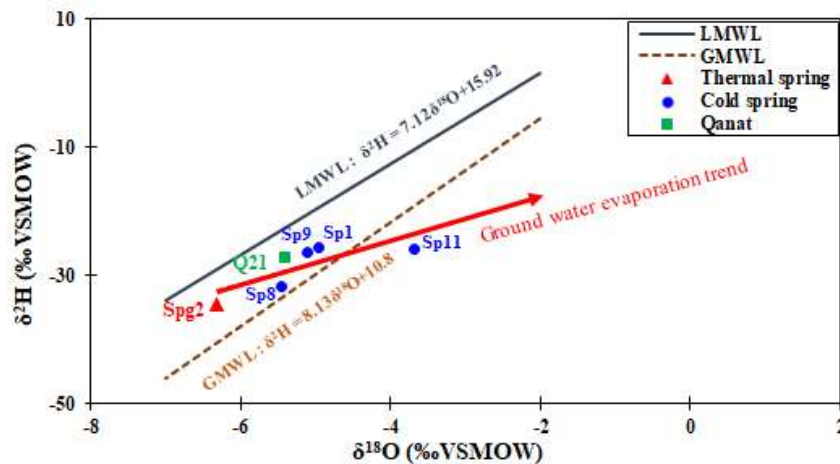


Figure 11. Stable isotopic composition of $\delta^2\text{H}$ and $\delta^{18}\text{O}$ in the groundwater and thermal spring, GMWL (Craig 1961) and LMWL (Jahanshahi and Zare 2017)

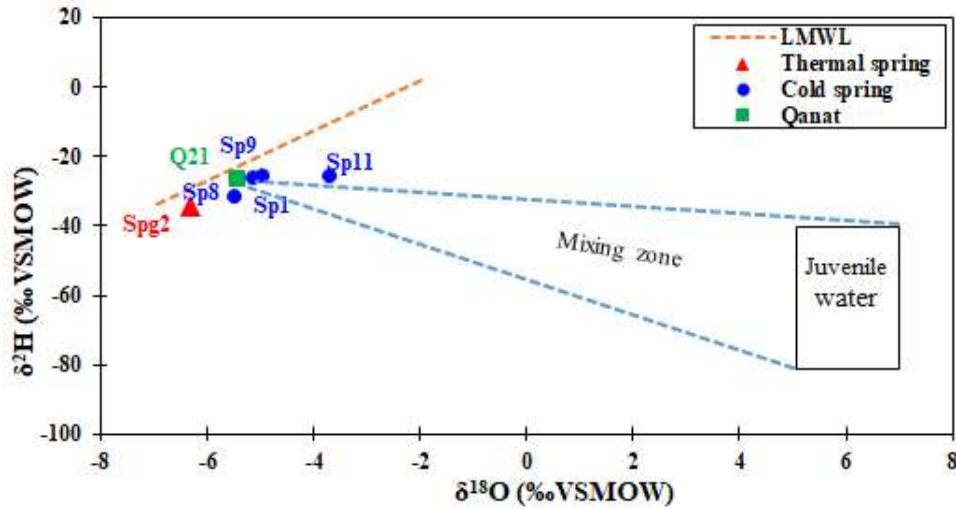


Figure 12. The possibility of effect of juvenile water on the thermal springs in the study area

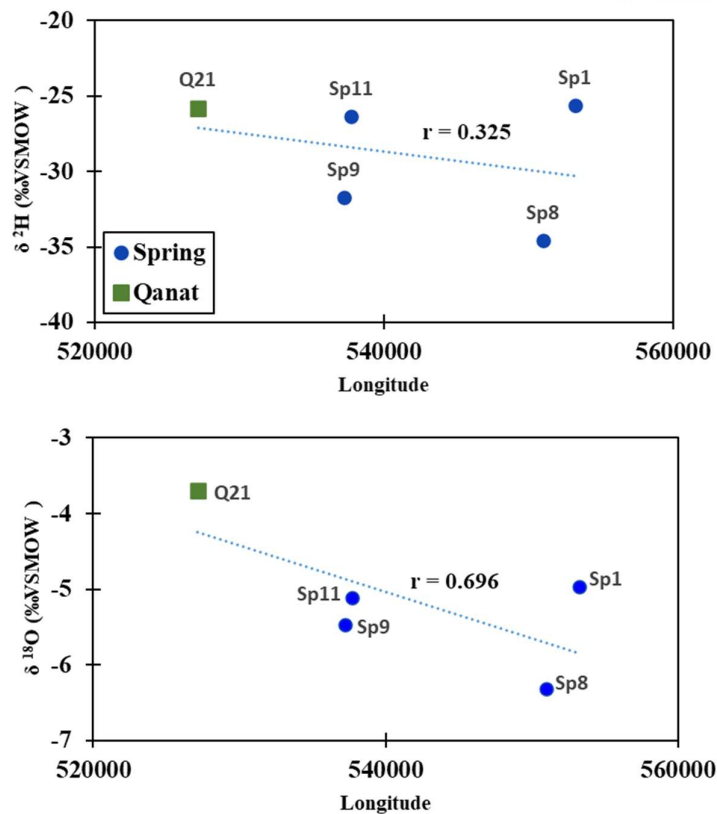


Figure 13. Relationship between isotopic composition and longitude of location of groundwater resources

According to Clark and Fritz (1997), at higher altitudes, where the mean temperature is low, precipitation and groundwater are isotopically depleted in $\delta^2\text{H}$ and $\delta^{18}\text{O}$. Considering the relationship between $\delta^{18}\text{O}$ and $\delta^2\text{H}$ and the elevation of the water sampling sites, it can be seen in Fig. 14a,b that, contrary to expectations, this relationship is positive or without a strong relationship. To investigate this issue, the mean topographic heights around the water sampling sites were considered (Fig. 14c,d). The diagrams showed that the spring Sp1 with the highest

altitude, had more enrichment which could be due to the source of recharge for this spring. This spring was located in the heights of Sarbijan mountain with the most elevation in the study area. In terms of precipitation, the most snow falls in this area, hence this region is mostly covered by snow. Since, the isotopic composition for snow is more enriched than rain, the recharged springs from snow (at higher altitude) had more enrichment compared to the springs at low altitudes. Among the water samples, spring Sp11 was also more isotopically enriched compared to other springs. In the outlet of this spring, the water flow was very low (about 1 L/s) and stagnant. It seems that as a result of low water velocity and high residence time at the earth's surface, the rate of evaporation and isotopic enrichment has increased.

Generally, with the increase of salinity in water due to evaporation, the composition of stable isotopes of $\delta^{18}\text{O}$ and $\delta^2\text{H}$ shows an enrichment trend (Clark and Fritz, 1997); while the relation of EC and major ions with the $\delta^{18}\text{O}$ and $\delta^2\text{H}$ had a decreasing trend in groundwater in the study area (Fig. 15). It seems that the type of precipitation in the recharge area has played an important role; because the springs related to snowmelt had lower EC and more enriched isotope. In general, there is a positive relationship between water temperature and the enrichment of stable isotopes of $\delta^{18}\text{O}$ and $\delta^2\text{H}$ (Clark and Fritz, 1997). In fact, with increasing temperature, the rate of evaporation from water increases, leading to isotopic enrichment, while in the study area this relationship is negative (Fig. 15), which could be due to that the fact the recharged springs from snow melt have lower temperature and more enrichment.

Groundwater mixing model

In the study area, the probable role of water resources mixing in the hydrogeochemical evolution of groundwater was examined through a mixing model. To determine the number of end-members, the methodology of Scheiber et al. 2018, known as the End-Member-Mixing-Analysis (EMMA) was used. The physicochemical parameters of water samples, including temperature, EC, pH, and major ions were considered.

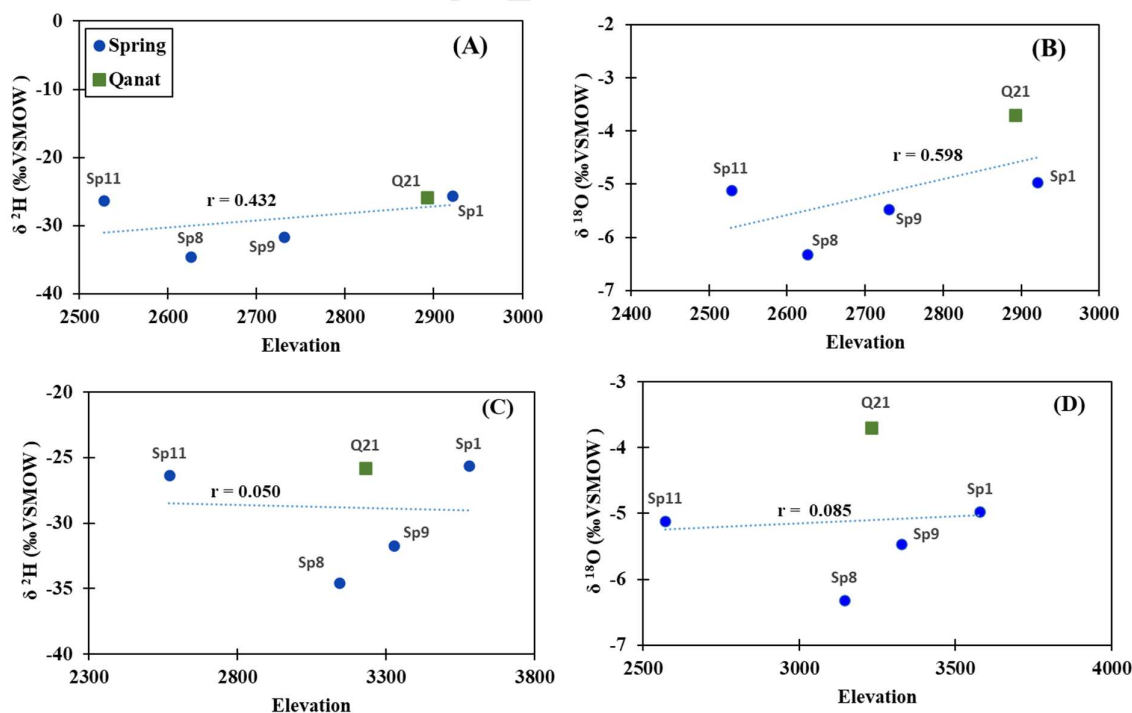


Figure 14. The relation of $\delta^{18}\text{O}$ and $\delta^2\text{H}$ with altitude of water samples

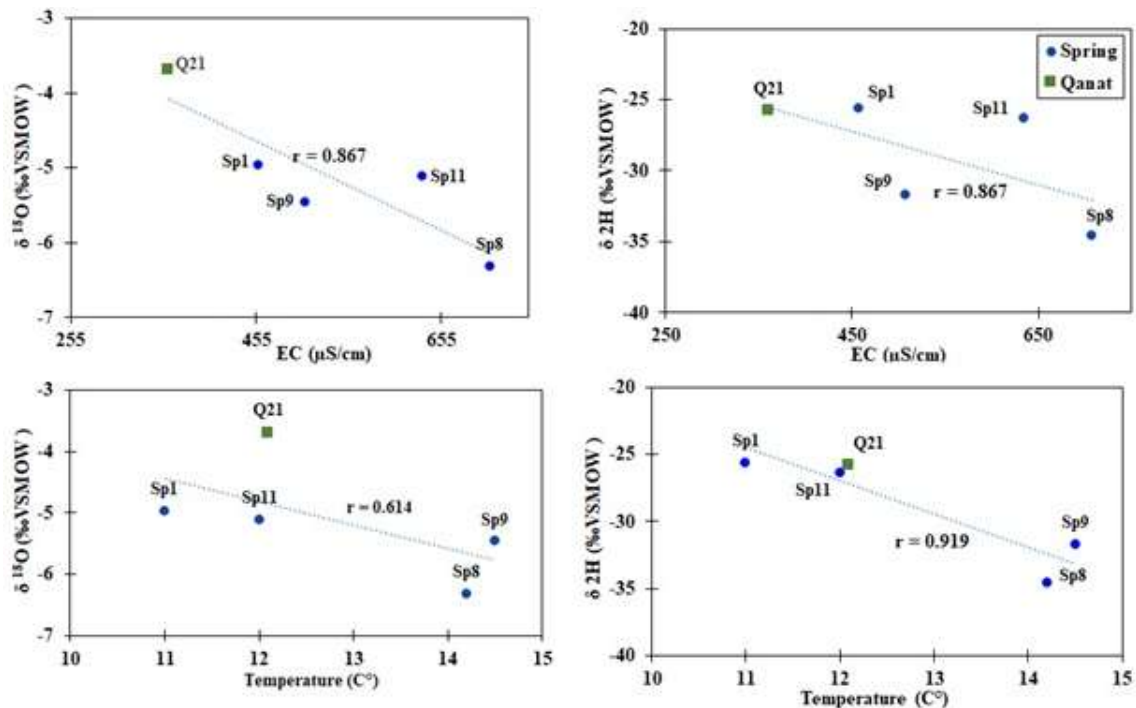


Figure 15. The relationship of $\delta^{18}\text{O}$ and $\delta^2\text{H}$ with EC and temperature

The results indicated that three end-members (samples of Q6 with highest EC, SP3 with lowest EC, and R4 representing surface water) were needed to explain 85% of the variability in the hydrochemical composition of the water samples. The percentage of each end member (Q6, SP3 and R4) in the groundwater resources was estimated in the study area (Fig. 16). Overall, the results showed that water sample Q6 had the highest percentage of mixing in the water resources, with its percentage decreasing in the north of the study area. The percentage of the mixing end member SP3 in the groundwater resources increased in the north and northwest of the study area. Finally, as the river was a gaining stream in the study area, it was observed that the river water had the least contribution to the evolution of the groundwater resources.

Geothermometry

According to the chemical geothermometers Na-K-Ca and Na-K for the two hot springs, the temperature of the thermal reservoir is estimated at 79.10 and 71.77 °C, respectively (Table 2). Moreover, using modeling to calculate mineral saturation indices in the hot springs at various temperatures, the equilibrium temperature, which is equivalent to the temperature of the heat reservoir, was determined (Fig. 17). This method showed that the mineral saturation indices for both hot springs equilibrate at 80 °C, which is close to the calculated temperature via the Na-K-Ca geothermometer.

To evaluate the chemical balance of the hot springs and their suitability for estimating reservoir temperature, a triangular diagram Na-K-Mg (Giggenbach, 1988) has been used. The composition of water is obtained from water-rock interaction as a function of temperature (Giggenbach and Glover, 1992). According to the Giggenbach diagram, immature and balanced waters in thermal reservoirs can be distinguished. The plotted points of thermal springs in the study area on the Giggenbach diagram in Fig. 18 showed that these hot springs were on the equilibrium line. Therefore, the estimated temperature of the thermal reservoir in the study area based on the Mg-K geothermometer is calculated to be about 280°C, which is higher than the

estimated temperature by the Na-K geothermometer. It seems that the concentration of Mg is high which results from water-rock interaction and has been diluted via CO₂ uptake and oxidation, or immature water. Therefore, the CCG method (Niva and Niva, 1987) has been used to correct the amount of magnesium. Since the amount of magnesium in thermal waters is high, the temperature calculated by other geothermometers may not be reliable. To address this issue, the CCG method (Niva and Niva, 1987) is used to calculate the equilibrium temperature in the study area. Using the CCG method, the temperatures of the thermal reservoir for the hot spring Spg1 and Spg2 were calculated to be 165 and 164.5 °C respectively. It should be noted that in some cases, geothermometric calculations may not be accurate due to hydrological conditions not matching basic calibration and geothermometric assumptions. However, the results show that the calculated temperatures from geothermometers are not consistent, which could be due to the mixing of cold water with deep water or synthetic chemical reactions in geothermal reservoirs.

Table 2. Estimated temperature of thermal reservoir according to chemical geothermometers

Sample	Sample (T°C)	Na-Ca-k $\beta = 4/3$	(Na/k) (Truesdill, 1976)
SPg1	45.9	79.10	71.77
SPg2	48.8	79.10	71.77

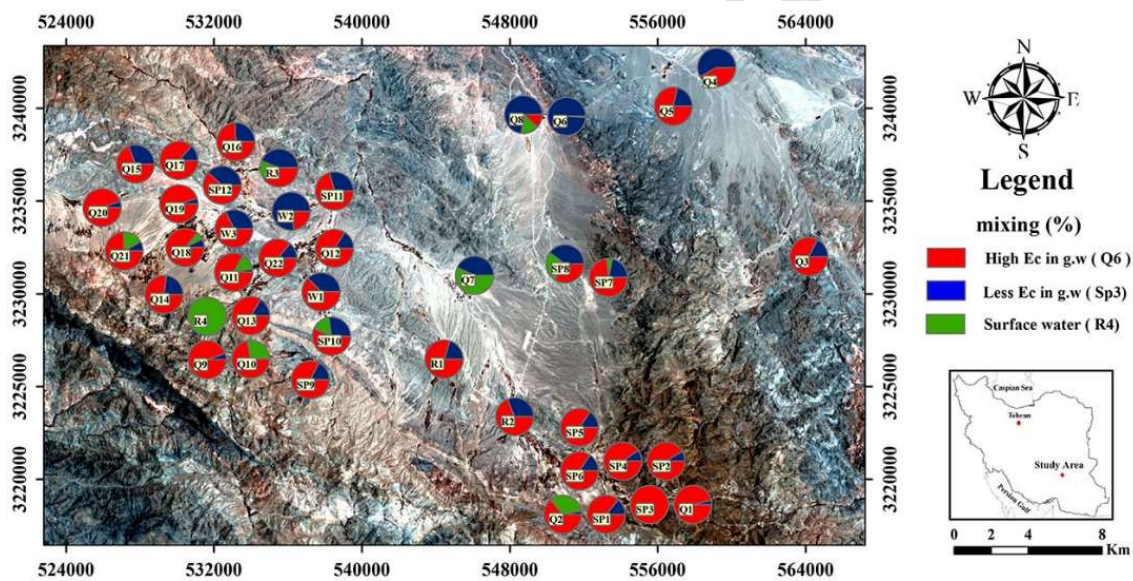


Figure 16. The distribution map of groundwater resources mixing in the study area

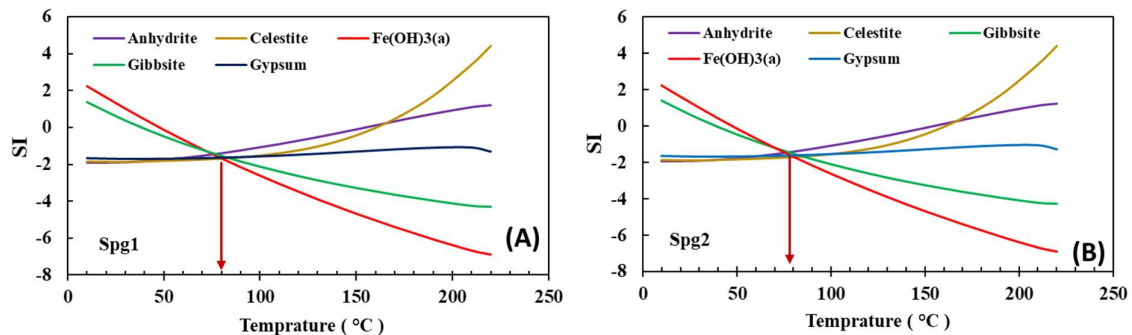


Figure 17. Diagrams of the mineral equilibrium of hot springs Spg1 and Spg2

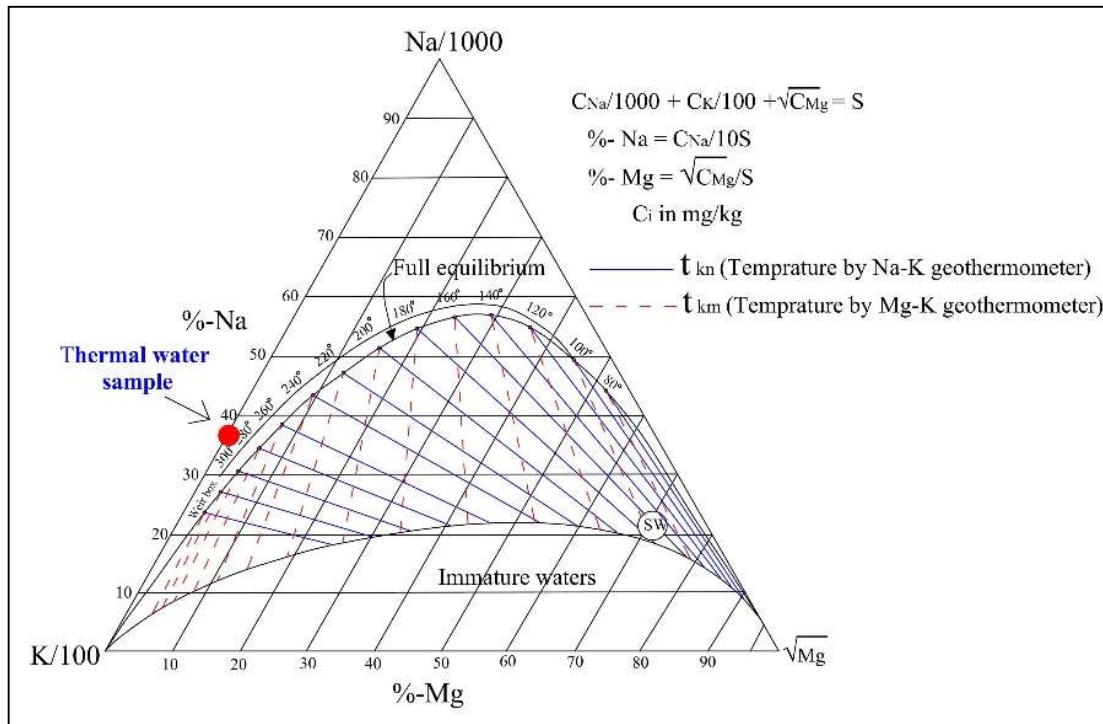


Figure 18. Triangular diagram of Na-K-Mg (after Giggenbach, 1988) for the thermal spring sample in the study area

To determine the depth of circulation of hot spring water in the study area, Equation 3 has been used (Askari Malekabad et al. 2020).

$$D = (T - T_0) / G \quad (3)$$

Which, D is the thermal reservoir depth (m), T is the equilibrium thermal reservoir temperature (°C), T_0 is the hot spring temperature (°C) and G is the geothermal gradient in °C.

In general, the natural geothermal gradient is 3°C per 100 meters. Of course, the presence of volcanoes in any region indicates that the geothermal gradient is greater than normal. The maximum possible gradient for the geothermal zone in the continental crust is 4.6 °C per 100 m (Sutherland et al., 2017). According to the average temperature of 47.35 °C in two hot springs and average of the estimated temperatures in the thermal reservoir (165 °C), the depth of the thermal reservoir was estimated at 3.92 and 2.5 km via the natural gradient and the proposed gradient of Sutherland et al. (2017) respectively.

Conclusion

In this area most groundwater samples were supersaturated with respect to calcite and dolomite, indicating that the groundwater has reached a thermodynamic equilibrium with respect to these two minerals. While all samples were undersaturated with respect to gypsum and halite, which indicates that parts of the groundwater where these minerals were abundant affect the chemistry of groundwater. According to the ionic ratios, it is observed that calcium can also be obtained from sources other than calcite from the dissolution of minerals such as gypsum, dolomite and silicates, and calcium in some groundwater sources was most likely removed from the solution by sedimentation or ion exchange. In addition to the dissolution of halite, the origin of sodium can be due to the weathering reaction of silicates and cation exchange. According to the results of cluster analysis, the study area was divided into three clusters. Samples of Cluster 1 had Na-

SO₄, Na-HCO₃, Ca-HCO₃, Na-Cl type, and cluster 2 and 3 had Ca-HCO₃ type. According to the results of chemical analysis in the west of the region, the amount of bicarbonate was higher and the pH was the lowest. Probably the presence of carbonate formations in the west of the region had increased the amount of bicarbonate in the water. The calculated carbon dioxide pressure in the groundwater of the study area was higher than the carbon dioxide pressure in the air. Considering this, it is not possible to comment on the close or open of the aquifer. The hot springs in the region showed a different chemical composition than other samples and had the highest electrical conductivity and sulfate content. The origin of the sulfate in the hot springs was not related to gypsum, it is probably from the evaporated mineral mirabolite. This layer in the basement may be a thin layer or the water path through this layer in the basement is small. Chemically, the two hot springs were of the Na-SO₄ type. According to isotopic studies, the origin of cold water springs and qanats in the study area was the rainfall in the area, and the origin of hot water springs in the study area was probably the current atmospheric water. According to the studies conducted, it is likely that re-evaporation from precipitation had occurred in the area. Considering the average isotopic composition of precipitation and magmatic waters and the mixing range between them, the formation of cold water springs, hot water springs, and qanats due to mixing was low. According to the results and the relationships between $\delta^2\text{H}$, $\delta^{18}\text{O}$ values with EC, longitude, altitude and temperature, it can be said that the Sp1 spring, which was located in the southwest of the region and had the highest altitude, showed greater enrichment, which may be due to more snowfall in this area, and also due to heavy snowfall, the snow retention time and snow melting time were longer. Given that the isotopic composition of snow is richer than that of rainwater, in this region, snow-recharge springs at higher altitudes had a richer isotopic composition compared to rain-recharge springs at lower altitudes. According to the Gigenbach diagram, the hot springs were located close to the perfect equilibrium line with a temperature of approximately 280°C. According to the CCG method, the reservoir temperature was 165°C and the depth of the thermal reservoir was probably 2500-3900 m from the surface.

References

- Aghazadeh, N., Chitsazan, M., Golestan, Y., 2017. Hydrochemistry and quality assessment of groundwater in the Ardabil area, Iran. *Applied Water Science*, 7: 3599-3616.
- Ahmadi, S., Jahanshahi, R., Moeini, V., Mali, S., 2018. Assessment of hydrochemistry and heavy metals pollution in the groundwater of Ardestan mineral exploration area, Iran. *Environmental Earth Sciences*, 77(5): 212.
- Aly, A.A., 2015. Hydrochemical characteristics of Egypt western desert oases groundwater. *Arab J Geosci*, 8: 7551-7564.
- Askari Malekabad, F., Jahanshahi, R., Bagheri, R., 2020. Characterization of the Bazman geothermal field, the southeast of Iran. *Geopersia*, 10 (2): 405-418.
- Bagheri, R., Nadri, A., Raeisi, E., Eggenkamp, H.G.M., Kazemi, G. A., Montaseri, A., 2014. Hydrochemical and isotopic ($\delta^{18}\text{O}$, $\delta^2\text{H}$, $^{87}\text{Sr}/^{86}\text{Sr}$, $\delta^{37}\text{Cl}$ and $\delta^{81}\text{Br}$) evidence for the origin of saline formation water in a gas reservoir. *Chemical Geology*, 384: 62-75.
- Bahadori, D., Jahanshahi, R., Dehghani, V., Mali, S., 2019. Variations of stable oxygen and hydrogen isotope ratios in the cold and thermal springs of the Bazman volcanic area (in the southeast of Iran). *Environmental Earth Sciences*, 78: 663.
- Clark, I.D., Fritz, P., 1997. *Environmental Isotopes in Hydrogeology*. Lewis Publishers, 342 pp.
- Craig, H., 1961. Isotopic variations in meteoric waters. *Science*, 133(3465): 1702-1703.
- Dimitrijevic, M.D., 1973. *Geology of Kerman region*. Geological Survey of Iran, Report 52, 334 pp. discriminate tectonic setting in VMS environment. *Economic Geology*, 97(3): 629-642.
- Drever, J., 1988. *Geochemistry of Natural Waters 2nd Edition*. Prentice Hall, 437 pp.
- Ehya, F., Marbouti, Z., 2016. Hydrochemistry and contamination of groundwater resources in the Behbahan plain, SW Iran. *Environ Earth Sci*, 75: 455.

- Giggenbach, W.F., 1988. Geothermal solute equilibria. Derivation of Na-K-Mg-Ca geoindicators. *Geochimica et Cosmochimica Acta* 52(12): 2749-2765.
- Giggenbach, W.F., Glover, R.B., 1992. Tectonic regime and major processes governing the chemistry of water and gas discharges from the Rotorua geothermal field, New Zealand. *Geothermics* 21(1): 121-140.
- Giridharan, L., Venugopal, T., Jayaprakash, M., 2008. Evaluation of the seasonal variation on the geochemical parameters and quality assessment of the groundwater in the proximity of River Cooum Chennai India. *Environ Monit Assess*, 143: 161-178.
- Jacintha, T.G.A., Rawat, K.S., Mishra, A., Singh, S.K., 2016. Hydrogeochemical characterization of groundwater of peninsular Indian region using multivariate statistical techniques. *Applied Water Science*, 7: 3001-3013.
- Jahanshahi, R., Zare, M., 2017. Delineating the Origin of Groundwater in the Golgohar Mine Area of Iran Using Stable Isotopes of ^2H and ^{18}O and Hydrochemistry. *Mine Water Environ*, 36: 550-563.
- Loh, Y.S.K., Akurugu, B.A., Manu, E., Aliou, A., 2020. Assessment of groundwater quality and the main controls on its hydrochemistry in some Voltaian and basement aquifers, northern Ghana. *Groundwater for Sustainable Development*, 10: 100296.
- Mali, S., Jafari, H., Jahanshahi, R., Bagheri, R., 2022. Groundwater Source Identification and Flow Model of the Dareh-Zar Copper Mine in Central Iran by Chemo-isotopic Techniques. *Mine Water and the Environment*, 41(4): 921-937.
- Nakhaie Sarvedani, B., Jahanshahi, R., Assari, A., 2022. Determining the best places for dewatering wells in the Gohar-Zamin pit mine, using geostatistical methods. *Geopersia*, 12(2): 287-298.
- Nieva, D., Nieva, R., 1987. Developments in geothermal energy in Mexico-Part Twelve. A cationic geothermometer for prospecting of geothermal resources. *Heat Recovery Systems & CHP*, 7(3): 243-258.
- Ohmoto, H., 1986. Stable isotope geochemistry of ore deposits. *Rev Mineral*, 16: 491-560.
- Scheiber, L., Ayora, C., Vázquez-Suñé, E., 2018. Quantification of proportions of different water sources in a mining operation. *Sci Total Environ*, 619-620, 587-599.
- Sethy, S.N., Syed, T.H., Kumar, A., Sinha, D., 2016. Hydrogeochemical characterization and quality assessment of groundwater in parts of Southern Gangetic Plain. *Environ Earth Sci*, 75: 232.
- Shojaei Baghini, S., Jahanshahi, R., Mali, S., Nasiri, M.A., 2020. Destruction of groundwater quality and the risk of saltwater intrusion in the aquifers nearby Sirjan salt playa, Iran. *International Journal of Environmental Analytical Chemistry*, 100(6): 647-661.
- Sunkari, E.D., Abu, M., Bayowobie, P.S., Dokuz, U.E., 2019. Hydrogeochemical appraisal of groundwater quality in the Ga west municipality, Ghana: Implication for domestic and irrigation purposes. *Groundwater for Sustainable Development*, 8: 501-511.
- Sutherland, R., Townend, J., 2017. Extreme hydrothermal conditions at an active plate-bounding fault. *Nature*, 1546(7656): 137-140.
- Telahigue, F., Agoubi, B., Souid F., Kharroubi A., 2018; Assessment of seawater intrusion in an arid coastal aquifer, south-eastern Tunisia, using multivariate statistical analysis and chloride mass balance. *Phys. Chem. Earth. Parts A/B/C*, 106: 37-46.

